Rainfall thresholds for shallow landsliding derived from pressure-head monitoring: cases with permeable and impermeable bedrocks in Boso Peninsula, Japan

著者	Matsushi Yuki, Matsukura Yukinori
journal or publication title	Earth surface processes and landforms
volume	32
number	9
page range	1308-1322
year	2007-08
権利	(C) 2007 John Wiley & Sons, Ltd.
URL	http://hdl.handle.net/2241/91523

doi: 10.1002/esp.1491

Rainfall thresholds for shallow landsliding derived from pressure-head monitoring: cases with permeable and impermeable bedrocks in Boso Peninsula, Japan

Yuki Matsushi *, Yukinori Matsukura

Geoenvironmental Sciences, Graduate School of Life and Environmental Sciences, University of Tsukuba, Japan

**Correspondence to: Y. Matsushi, Present address: Applied Accelerator Division, Research Facility Center for Science and Technology, University of Tsukuba, Tenno-dai 1-1-1, Tsukuba, Ibaraki 305-8577, Japan.*

E-mail: matsushi@tac.tsukuba.ac.jp

Tel.: +81-29-853-4461; Fax: +81-29-853-2565.

Abstract

Rainfall thresholds for shallow landslide initiation were determined for hillslopes with two types of bedrocks, permeable sandstone and impermeable mudstone, in the Boso Peninsula, Japan. The pressure head response to rainfall was monitored above a slip scarp due to earlier landslides. Multiple regression analysis estimated the rainfall thresholds for landsliding from the relation between the magnitude of the rainfall event and slope instability caused by the increased pressure heads. The thresholds were expressed as critical combinations of rainfall intensity and duration, incorporating the

geotechnical properties of the hillslope materials and also the slope hydrological processes. The permeable sandstone hillslope has a greater critical rainfall and hence a longer recurrence interval than the impermeable mudstone hillslope. This implies a lower potential for landsliding in sandstone hillslopes, corresponding to lower landslide activity.

Keywords: shallow landslides; hillslope hydrology; slope stability; pressure head; critical rainfall

Introduction

Extreme precipitation causes shallow landsliding of soil-mantled steep hillslopes in humid temperate regions. Catastrophic landslides remove material from hillslopes and scour low-order channels, supplying large quantities of sediment to high-order fluvial systems. Rainfall-induced landslides pose a grave threat to lives and property, since the soil mass on hillslopes slips suddenly and often travels a long distance as a high-speed debris flow. These landslides cause thousands of deaths and serious economic damage world-wide, especially in mountainous regions subject to heavy rainfall.

The identification of rainfall thresholds for landslide initiation is a basic task in predicting and dealing with disasters. An initial concept of the rainfall threshold was developed by distinguishing between rainfall events that triggered landslides and storms that did not trigger landslides. Several researchers established empirical thresholds by identifying critical combinations of rainfall intensity and duration (Caine, 1980; Cannon and Ellen, 1985; Wieczorek, 1987; Terlien, 1998; Jakob and Weatherly, 2003).

Empirical thresholds can be applied in the issuing of landslide warnings, in combination with real-time monitoring of a network of telemetering rain gauges and regional precipitation forecasts (Keefer *et al*., 1987).

A weakness of empirical approaches is that they treat the subsurface physical processes as a 'black box'. The stability of hillslopes is affected by elevated pressure heads that reduce the soil shear strength. Traditional thresholds either ignore or inadequately account for slope hydrology and geotechnical properties of the slope materials. Process-based approaches may enable us to address the hydrological conditions and rainfall thresholds that lead to initiation of landslides.

Montgomery and Dietrich (1994) extended an infinite-slope stability analysis to incorporate steady-state saturated flow oriented parallel to the slope. However, hydrological observations taken during rainstorms contradicted the predictions of steady-state slope hydrology. Instead, soils on a landslide source area respond transiently to rainfall, and non-steady moisture redistribution follows the vertical rainwater infiltration (Johnson and Sitar, 1990; Fannin and Jaakkola, 1999; Fannin *et al*., 2000; Simoni *et al*., 2004).

Non-steady hydrological processes were modeled by Iverson (2000) in conjunction with the steady-state distribution of pressure heads as a pre-storm moisture condition. The model resolved the timescale discrepancy between the theoretical and real slope hydrology, and also introduced the representation of direct triggering of shallow landslides. D'Odorico *et al*. (2005) extended the model to evaluate critical intensities and frequencies of rainfall for landsliding.

Quantitative relations between slope materials, slope hydrology, and rainfall thresholds remain controversial. Soils on natural hillslopes mainly originate from decomposition of

bedrock, so that geological variation in the bedrock produces varying mechanical and hydrological properties in the soils. Consequently, the rainfall threshold depends on the geology of the hills. Indeed, the temporal and spatial frequency of shallow landslides varies with basin geology. Evaluation of the relation between the rainfall thresholds and hillslope composition will cast light on variation in landslide activity in diverse geological settings.

The present study aims to determine the site-specific rainfall thresholds in two hilly locations with contrasting morphology and bedrock. Detailed field and laboratory investigations were designed to ascertain the physical properties of the hillslope materials relevant to slope stability analysis, and to understand the responses of subsurface pressure heads to rainfall. A multiple regression analysis was used to determine the critical rainfall level for landsliding, depending on the amount of rainfall and slope instability caused by elevated pressure heads.

Study area and site description

General setting

The study area is located in the south-west of the Boso Peninsula, central Japan (Figure 1). The area exhibits distinct topographical characteristics that vary with hills in the northwest to the southeast. The hill terrain in the northwestern section exhibits relatively high rounded crests (relative relief of 150–200 m) with low drainage density (5–8 km^{-1}). The southeastern hills have low rugged ridges (relative relief of 50–100 m) with high drainage density (15–22 km^{-1}).

The bedrock in this area belongs to the middle Pleistocene forearc basin fill, characterized by repeated sandy and muddy depositional sequences (Ito, 1998; Ito and

Horikawa, 2000). Coarse sandstone and conglomerates (*ca*. 600–700 ka) comprise the northwest high terrain, whereas muddy sandstone and sandy mudstone (*ca*. 700–800 ka) make up the southeastern lower terrain. Hereafter, we refer to these two areas as the sandstone area and the mudstone area (Figure 1B).

The region has a humid temperate climate with average daily temperatures between 5 °C and 30 °C, and with a mean annual rainfall of 1500–2000 mm. Seasonal fronts in early summer and fall, as well as occasional typhoons, contribute 40–50% of the total rainfall. The orographic effect slightly enhances rainfall in the southern part of the peninsula. The area receives very little snowfall, and the snow coverage rarely remains on the ground for extended periods.

A planted forest of cypress (*Chamaecyparis obtusa*) and cedar (*Cryptomeria japonica*) covers the majority of the study area. Hardwood and various understory species also coexist within the conifer stands. The forest age varies from several years to several decades. No large-scale timber harvesting has been conducted in recent decades.

Shallow landslides in the study area

The study area has experienced episodic landslide events caused by heavy rainstorms. Torrential rainfall on August 1, 1989 caused the largest landslide event in recent decades (Furuya and Ohkura, 1992). Four meteorological stations within a 30-km radius from the study area provided the rainfall records for the storm (see Figure 1A for their locations). The rainfall at the peak of the storm had an hourly intensity of 30–70 mm/h (Figure 2). The storm body provided cumulative rainfall of between 250 mm (observed at Yokohama) and 450 mm (observed at Sakuma) during the 24 hours following the onset of the storm.

The rainstorm produced many slides along the mudstone slopes, but only a few hillslopes failed in the sandstone area. The landslide density in the mudstone area reached 71·1 km^{-2}, about 19 times larger than that in the sandstone area (3·8 km^{-2}) (Matsushi *et al*., 2006). In the sandstone area, the landslides only occurred on the steep lower parts of hillslopes adjacent to major valleys, while the landslides in the mudstone area took place mainly on uppermost hollows near the slope crests (Matsushi and Matsukura, 2004).

Selection of the slipped slopes

A slipped slope was selected for investigation, with typical size and geometry in each area (Figure 1C, D). Figure 3 shows the profiles of the selected slopes. The slip scars on the slopes have a shallow platy form bounded by a small scar step, showing the general geometry of a translational landslide (Selby, 1993, pp.260–263). The landslides on the sandstone slope were 1·2–1·8 m in depth, 35–40° in slope angle, and ~10^3 m^3 in sliding volume, which were deeper, steeper, and larger than those on the mudstone slopes (0·6–0·9 m, 30–35°, and ~10^1 m^3). These landslides seem to have resulted from the 1989 storm, since they were first observed in an aerial photograph taken in 1990.

The subsurface structures of the slopes were determined by taking soil soundings along the scar profiles, using a simplified dynamic cone penetrometer (MARUTO Testing Machine Co., Japan). The thickness of the soil mantle is defined as the depth at which the penetrating resistance, $N_c = 30$, where the value of N_c is the number of cone impacts needed to penetrate 10 cm. The soil on the sandstone slope developed to 6–7 m at the point of greatest thickness (Figure 3). The slip plane of the landslide is perched within the thick soil layers. However, the soil on the mudstone slope forms a relatively thin

veneer of up to a meter deep over the bedrock (Figure 3). The slip plane lies immediately above the sharp soil–bedrock boundary.

Slope materials

Soil pits were dug at the scar heads in order to obtain undisturbed soil samples for geotechnical tests. The samples were used to obtain the dry unit weight of soils, porosity, grain-size distribution, and saturated hydraulic conductivity through the shallow soil profiles. These soil properties were reported previously in Matsushi *et al*. (2006). Shear strengths were measured using soil specimens in which the moisture contents were adjusted stepwise from oven-dried to capillary saturated conditions. Matsushi and Matsukura (2006) formulated shear strength reduction due to soil wetting as a function of the volumetric water content of the soils.

Table I summarizes the geotechnical soil properties. The soil on the sandstone slope has a greater unit weight and a smaller porosity than the soil from the mudstone slope, which reflects the grain-size distribution of the soils. The soils originating from sandstone contain a large fraction of sand particles (>80%), whereas the soils originating from mudstone contain finer material, with more than 50% accounted for by silt and clay (Table I).

The permeability of the soil on the sandstone slope is in the order of 10^{-5} m/s, and exhibits no hydraulic discontinuity through the soil layer down to the bedrock. The permeability of the sandstone bedrock exceeds the magnitude of maximum rainfall intensities in the study area (Matsushi *et al*., 2006), so the incoming rainwater is able to percolate deep into the hillslope. In contrast, the permeability in the mudstone slope decreases significantly with depth. Permeabilities of 10^{-5}–10^{-6} m/s observed in the

shallow soil fall abruptly to 10^{-8} m/s at the bedrock. Consequently, infiltrated rainwater accumulates upon the impermeable bedrock during intense rainstorms.

The characteristics of decline in soil shear strength with increasing moisture content are given by the following equation (Matsushi and Matsukura, 2006):

$$\tau = C\mathrm{e}^{-\mu\theta} + \sigma \tan\phi \tag{1}$$

where, τ is the shear strength, C is the apparent maximum soil cohesion at dry condition, μ is the reduction coefficient, θ is the volumetric water content, σ is the normal stress, and ϕ is the angle of shearing resistance. Equation 1 indicates an exponential decrease in the cohesive strength with increasing soil moisture, with the optimum parameter values listed in Table I.

The soil-water characteristic curve (SWCC) was determined by taking undisturbed soil cores from depths of 30 and 75 cm in the sandstone pit, and depths of 15 and 30 cm in the mudstone pit. The samples were left for at least 48-h in a water-filled container to ensure capillary saturation. The drying SWCC was then measured using the water head method with a range of pressure heads from 0 to −0·6 m, and the vacuum method from −0·6 to −3·9 m (Figure 4).

The broken and solid lines in Figure 4 show the best-fit model curves. An equation of van Genuchten's (1980) model as modified by Kosugi (1994) was adopted:

$$\theta = \theta_{\mathrm{r}} + \left(\theta_{\mathrm{s}} - \theta_{\mathrm{r}}\right)\left[1 + m\left(\frac{\psi}{\psi_0}\right)^{\frac{1}{1-m}}\right]^{-m} \tag{2}$$

where θ_s is the saturated volumetric water content, θ_r is the residual volumetric water content, ψ is the pressure head, ψ_0 is the pressure head at the inflection point of the model curve, and m is a fitting parameter ($0<m<1$). In this case, the air-entry value of the soil is assumed to be zero, because the specimens drain gravitational water promptly after the onset of negative pressure heads (Figure 4).

The value of θ_s was fixed as the volumetric water content at the zero-pressure head for each of the soils, while the other parameters (i.e. θ_r, ψ_0 and m) were estimated by non-linear least squares optimization. The fitting analysis provided the optimum parameter values in Table II. The values accurately represent the observed soil-water retention characteristics (r^2 = 0·98 and 0·95 for the soils originating from the sandstone, 0·95 and 0·99 for those from the mudstone, see also Figure 4).

Slope hydrology

Methods of hydrological observation

The hydrological responses of the soils to rainfall were observed, focusing on the pressure head and volumetric water content. Simultaneous monitoring of these parameters enables us to draw an 'in situ' SWCC including hysteresis between the drying and wetting processes of the soils. Therefore, the in situ curve makes it possible to estimate the ranges of alteration in the 'laboratory' parameters.

Tensiometers with pressure transducers (RSUxx, IRROMETER Co., USA) were set up at 2·0 m upslope from the scar heads to monitor subsurface pressure heads (Figure 3). All of the tensiometers were calibrated at the laboratory before installation to within ± 0·01 m precision. The nest of tensiometers was established with monitoring depths of 30,

75, and 120 cm on the sandstone slope, and of 30, 60, and 90 cm on the mudstone slope. A data logger connected to the pressure transducers recorded the subsurface pressure heads every 10 minutes.

A soil moisture sensor (ThetaProbe TYPE ML2x, Delta-T Devices Ltd., UK) was installed at each of the tensiometer nests to monitor the volumetric water content at 75 cm depth for the sandstone nest and 60 cm depth for the mudstone nest (Figure 3). The outputs from the sensor, the dielectric constants of soil, were collected with a data logger in 10-minute intervals. These were converted to volumetric water content with an accuracy of ± 0·02 m^3/m^3 by a laboratory calibration using undisturbed materials extracted from the monitoring depths.

Rainfall was also measured at 10-minute intervals with a tipping-bucket rain gauge placed in an open site on the forested slopes. The gauge has an orifice diameter of 20 cm, and stands approximately 60 cm above the forest floor. The recorded bulk rainfall was free from interception by surrounding understory vegetation, but may have been slightly influenced by projecting tree canopies.

The pressure heads and rainfall were observed from May 2004 to August 2005. The data of volumetric water content are available for the last six months, from February to August 2005. All of the observations included temporal respites during extremely dry periods, and downtimes when the loggers were filled up with data.

Pressure head fluctuations in shallow soil layers

The sandstone slope tended to maintain negative values for the pressure heads throughout the observation period (Figure 5A). The pressure heads momentarily exceeded 0 m only at the shallowest monitoring depth during rainfall peaks. The

pressure heads at the deeper points (depths of 75 and 120 cm) showed only a small range of fluctuations of up to −0·2 m, even during intense rainfall events.

The pressure heads on the mudstone slope reached positive values in response to almost all rainfall events at every monitored depth (Figure 5B). The positive pressures persisted for several hours to several days, indicating a build up of a transient water table on the bedrock. A marked decrease in the pressure heads followed irrigation intervals, especially in dry seasons. The pressure heads varied over a wide range during the summer months, from negative values of −3 m to positive values up to 0·5 m.

In situ soil-water retention characteristics

The observed volumetric water content plotted against the simultaneous pressure head measurements indicates the 'in situ' soil-water retention characteristics (Figure 6). The best-fit model curves for the laboratory data (Figure 4, Table II) are also presented in the diagrams (the solid and broken thin lines). The diagonal gray lines across the plots represent the envelopes covering the gap between the drying laboratory curves and the in situ-observed SWCCs. The parameter values for these envelopes are listed in Table II.

In the case of the sandstone slope, the upper edge of the in situ plots corresponds closely to the drying curves (Figure 6A). The in situ volumetric water contents were ~0·1 m^3/m^3 lower than for the drying curves, and the envelope for the plots covers the range of hysteresis between the soil drying and wetting processes.

In the case of the mudstone slope, the in situ SWCC differs markedly from the laboratory curves (Figure 6B). Although the laboratory curves and the in situ data exhibit similar trends with a near-zero pressure head, the in situ data exhibits a more water-retentive trajectory towards drying. This may result from disparities in soil texture

through the soil profile, between the shallower sampling points used for the laboratory tests (15 and 30 cm deep) and the deeper zone used for the in situ observation (60 cm deep). The upper envelope of the plots covers such spatial variance in the soil-water retention characteristic, rather than the wetting–drying hysteresis.

Discussion

Slope stability analysis

An infinite-slope model was employed to analyze the stability of the slopes, since the depth of past landslides is much smaller than their width or length (Figure 3). The analysis neglects all forces not resolvable on a potential failure plane that runs parallel to the ground surface. Reinforcement by piling and lateral tree roots was also not taken into account, as the major root systems were found to be above the actual slip depths.

In a limited equilibrium analysis, materials on a potential failure plane in an elongated slope are subject to two opposing forces: a downslope component of soil weight as a driving force, and the shear strength of the soil providing a resisting force. Three instability factors were taken into account: (1) reduction of soil cohesion in response to soil wetting, (2) weight increase of soil resulting from water absorption, and (3) decrease in effective stress derived from a positive pressure head. The first two were considered only in an unsaturated state, whereas the third factor is only relevant when the soil becomes saturated.

Assuming equable wetting of homogeneous soil and reduction in soil cohesion as described by Equation 1, the dimensionless factor of safety, *FS*, balances the driving and resisting forces as:

$$FS = \frac{\tan\phi}{\tan\beta} + \frac{Ce^{-\mu\theta}}{(\gamma_d + \theta\gamma_w)Z\sin\beta\cos\beta} - \frac{\mathrm{Max}(\psi, 0)\gamma_w \tan\phi}{(\gamma_d + \theta\gamma_w)Z\sin\beta\cos\beta} \quad (3)$$

where Z is vertical soil depth, β is slope angle, γ_d is the dry unit weight of soil, and γ_w is the unit weight of water (9·8 kN/m^3). When *FS* reduces below unity, the slope fails along the potential failure plane. Substitution of Equation 2 into 3 generates the factor of safety mediated by the pressure head, and allows us to follow fluctuations in slope stability under both unsaturated and saturated conditions.

The factors of safety were calculated from the observed pressure head at each monitoring depth with the local slope angles (38·8° for the sandstone slope, 35·7° for the mudstone slope). Two sets of parameters for the SWCC were used in the calculation: the set for the deeper samples in each of the soils as a representative of the laboratory curves (depth of 75 cm for the sandstone, and depth of 30 cm for the mudstone), and the set for the in situ envelopes (Table II). The other input-variables in the equations were assumed not to vary with depth, being fixed on the values in Table I.

In the sandstone slope, the factors of safety using the laboratory and in situ parameters for the SWCC show similar temporal variation (Figure 7A, B). The *FS*-values at 30 cm depth in the sandstone slope fall sharply from 6·0–4·0 to nearly 2·0 for each rainfall event, whereas those at depths of 75 and 120 cm respond less strongly and with a narrower range of fluctuations (*FS* = 3·0–1·0). The sensitive responses in the shallow zone are due to soil wetting from the land surface, and the subsequent water redistribution causes the instability in the deeper zones.

In the mudstone slope, the changing patterns of *FS* differ, depending on the SWCC

parameters used. The factor of safety fluctuates within a relatively wide range at all of the monitoring depths when using the laboratory parameters: $FS = 7{\cdot}0–2{\cdot}0$ for the 30 cm depth, $4{\cdot}0–1{\cdot}0$ for the depths of 60 and 90 cm (Figure 7C). However, the value of *FS* when using the in situ parameters exhibit a relatively narrow range of fluctuations, especially in the months from winter to spring (Figure 7D). The small *FS* fluctuations may result from the water-retentive tendency of the in situ SWCC (Figure 6B). Nevertheless, in both cases, positive pressure heads cause a reduction in *FS*-values to close to the stability limit of $1{\cdot}0$ under completely saturated conditions. Hence the disparity between the laboratory and in situ parameters does not affect the eventual destabilization of the mudstone slope.

Analysis of the relation between rainfall and slope instability

Individual rainfall events render the slope unstable, producing a transient decline in *FS*-values (Figure 8A). The relationship between the magnitude of the rainfall events and the minimum *FS*-values was analyzed at the deepest monitoring depths; 120 cm for the sandstone slope and 90 cm for the mudstone slope. These depths are located roughly on an extension of the actual slip surfaces (Figure 3). To evaluate the effect of hysteresis in soil wetting, the analysis for the sandstone slope was performed for both sets of *FS*-values, from the laboratory and in situ SWCCs. In the case of the mudstone slope, this dual analysis is not needed because the minimum *FS*-values appear under completely saturated conditions.

The temporal depression of the *FS*-value develops subsequent to the rainfall peak (Figure 8A). Rainfall patterns over a specified time period prior to the appearance of the *FS* dip affect the minimum *FS*-values. Therefore, the mean rainfall intensities during the

preceding x hours were calculated for every rainfall event; where x is a series of 28 time frames: 0·5, 1, 2, 3, 4, 5, 6, 8, 10, 12, 14, 16, 18, 20, 24, 30, 36, 48, 60, 72, 84, 96, 108, 120, 132, 144, 156, and 168 h.

The relationships between the minimum *FS*-values and the mean rainfall intensities were examined sequentially through the 28 preceding time frames (Figure 8B). The minimum *FS*-value for each of the instability events correlates inversely to the mean intensity of the preceding rainfall. The correlation becomes strongest at rainfall duration x_i h, indicating that x_i-h rainfall reduces the factor of safety most effectively.

The changes in the correlation coefficients rise with a peak at x_i-h rainfall duration (Figure 8C). A certain significant level (S.L.) statistically classifies effective and ineffective rainfall durations. In a linear-regression analysis, coincidence of a regression function for a certain dataset can be tested by the magnitude of the correlation coefficient, $|r|$. A probability, P, gives the quantitative likelihood of the regression function, which is defined as the probability that the correlation coefficient for a set of independent variables exceeds the observed $|r|$ statistic (Taylor, 1997, pp. 224–226). If P exceeds a given α%, the correlation will be rejected at the α% significant level. In the present study, the effective durations of rainfall were approved by the S.L. at which the P-value falls below 0·001%.

The relations between the minimum *FS*-values and the mean rainfall intensities in the effective durations provide statistically significant regression functions (Figure 8D). The critical rainfall for the stability limit is defined by an intersection of the linear-regression line and the horizontal line of $FS = 1{\cdot}0$. The value of the critical rainfall has an uncertainty range of $\pm 1\sigma$, using 68% confidence limits of the linear regression. Landsliding is expected when the mean rainfall intensity reaches the critical level within

a given effective duration.

A total of 24 events were collected for the regression analysis for the sandstone slope (Figure 9A). The regression coefficients for the varying rainfall durations show diphasic changes for both of the analyses using the in situ (triangles) and laboratory parameters (open circles) for the SWCC (the inset of Figure 9A). The first peak of the correlation arises at 14 h, and the slightly higher second one appears at 72-h rainfall duration. The analyses provide the two critical mean intensities in the 72-h rainfall duration, 3·4 mm/h (range of $\pm 1\sigma$ = 2·9–4·1 mm/h) for the in situ envelopes, and 2·6 mm/h (range of $\pm 1\sigma$ = 2·1–3·2 mm/h) for the laboratory curves. This strong correlation for the 72-h rainfall indicates that antecedent moisture conditions play a key role in the instability of the sandstone slope, particularly associated with rainfall for three days prior to an instability peak. The 14-h rainfall may be relevant as a direct trigger for shallow landsliding.

In the mudstone slope, the analysis of 49 events shows changes in the correlation coefficient with a single-peak pattern (the inset of Figure 9B). The correlation peak is at the 5h rainfall duration, which suggests that a comparatively short period of rainfall controls the slope destabilization. However, even in this case, antecedent moisture also contributes to slope instability. Antecedent moisture conditions may be the reason for the markedly-scattered plots in the regression for the mudstone slope. The critical rainfall for the duration of 5 h has the mean intensity of 14·3 mm/h (range of $\pm 1\sigma$ = 11·2–18·8 mm/h).

Critical combinations of rainfall intensity and duration

Statistically significant correlations were detected for the rainfall durations from 8 h to 84 h in the sandstone, and from 2 h to 16 h in the mudstone (Figure 9). The regression

analyses for all of these effective durations provide the discrete critical mean intensities of rainfall as plotted in Figure 10. The critical rainfall intensity, I, is a power-law function of rainfall duration, D:

$$I = 176.7D^{-0.91} \quad \text{(for the sandstone)}, \tag{4a}$$

$$I = 127.7D^{-0.89} \quad \text{(for the sandstone)}, \tag{4b}$$

$$I = 44.9D^{-0.70} \quad \text{(for the mudstone)}. \tag{4c}$$

Equations 4a and 4b correspond to the results from the in situ and laboratory SWCCs, respectively. The power-law correlation between the intensity and duration of critical rainfall accords with previously reported features of landslide-triggering thresholds (Caine, 1980; Cannon and Ellen, 1985; Wieczorek, 1987; Terlien, 1998; Jakob and Weatherly, 2003).

The critical rainfall intensities for the sandstone slope (open triangles and circles) are higher than those for the mudstone slope (solid circles). For example, the critical mean intensity of a 10-h rainfall is 9 mm/h for the mudstone, whereas the sandstone slope requires 15–20 mm/h for the same duration. Accordingly, landslides should occur on mudstone slopes with a smaller amount of rainfall than that required on sandstone slopes.

The two arrays of critical rainfall from the dual analysis for the sandstone slope exhibit a similar magnitude, but the results from in situ parameters (triangles) show slightly higher intensities than those from the laboratory (open circles). The in situ envelope of the soil-water retention involves wetting paths starting from a relatively dry condition,

whereas the laboratory one represents a drainage process from the saturated condition. Hence, the slight difference in the critical rainfall indicates the larger requirement of rainfall to attain slope instability from a drier condition.

The rainfall thresholds in this study can be verified from the records of the torrential rainfall on August 1, 1989, which caused landslides on the observed slopes. The four bold lines in Figure 10 indicate the temporal progress in mean rainfall intensity during the course of the storm. These lines were calculated from the records of cumulative rainfall at the four meteorological stations, divided by hours of elapsed time from the onset of the storm body (Figure 2). All the records showed that rainfall exceeded the analytical thresholds (Figure 10), which coincides with the fact that both the sandstone and mudstone slopes failed during the 1989 storm.

The larger critical rainfall for sandstone slopes predicts a delayed shallow landsliding. According to the records of the 1989 storm, the temporal progress in mean rainfall intensity crossed the mudstone threshold first, and then attained the sandstone threshold with a delay of a few to some tens of hours (Figure 10). Unfortunately, no record of actual landslide timings is available from the 1989 storm, so the validation of this prediction is left to future works which prove time-lags of the landslides within a prolonged storm event.

Recurrence intervals of critical rainfall

Rainfall records from 1940 to 2004 at Yokohama meteorological station provide standard intensity–duration–frequency curves of rainfall for the study area (solid lines in Figure 11). These curves were calculated by the specific coefficient method for the annual maximum records of 1-h and 24-h rainfall (Iwai and Ishiguro, 1970, pp.

162–177). The curves represent equipotential lines of probabilities (i.e. return periods) for varying combinations of rainfall intensity and duration.

By combining with the return periods of rainfall, one can translate the critical intensity–duration relationship to a recurrence interval of the landslide-triggering rainfall. The recurrence interval for critical rainfall ranges 3–200 years for the sandstone slope (incorporating the error bars), whereas it is 1·1–3 years for the mudstone slope (Figure 11). This refinement derives a minimum recurrence interval between landslide events, based upon an implicit assumption of optimal material conditions for failure at all times.

Of note is that sandstone slopes require higher rainfall intensity and greater rainfall duration to slide, and thus have longer return period of landslide events than mudstone slopes (Figure 11). The discrete recurrence intervals of critical rainfalls imply that the probability of landsliding varies from several to tens of times during a given time period. Longer recurrence intervals lead to lower potential for landsliding, and this corresponds to the lower landslide activity observed in the sandstone slopes (Matsushi *et al*. 2006).

Although rainfall in excess of the threshold is a necessary condition, it is not a sufficient condition for landslide initiation. Landslides do not occur in conditions of inadequate soil thickness. The thickness of soils on hillslopes changes both temporally and spatially, as old scars with different ages recover gradually with soil accumulation and bedrock weathering (Trustrum and De Rose, 1988; Reneau *et al*., 1990). Thus the spatial and temporal distribution of landslides is influenced strongly by the history of landsliding in the area (Iida, 2004).

Geotechnical properties of the slope material also change with time as the parent rock weathers and converts to soils. The effect of weathering becomes more prominent in

mudstone slopes, where the landslide-triggering storm has a shorter recurrence interval than a time-scale of bedrock weathering. In contrast, landslides on sandstone slopes seem to be controlled by the depth of wetting-front penetration in a significant rainfall event, because of the thick soil layers developing on the bedrock (Matsushi *et al*., 2006). Quantitative evaluation of actual landslide frequencies requires a more integrated approach incorporating numerical modeling of subsurface water behavior, basin wide distribution of soil thickness and its alteration over a long time-scale.

Conclusions

This study has focused on rainfall thresholds for landslide initiation from pressure head monitoring on two hillslopes underlain by permeable sandstone and impermeable mudstone in the Boso Peninsula, central Japan. An analysis of the relationship between the magnitude of rainfall and hillslope instability provides effective rainfall durations for slope instability. Three days of rainfall destabilizes the sandstone hillslope most effectively, which suggests the significance of ancient soil moisture for landslide initiation. For the mudstone hillslope, relatively short rainfall, with durations from several hours to half a day, is sufficient for slope instability. This indicates that intense and sudden rainfall contributes to triggering shallow landslides in mudstone hillslopes.

The critical rainfall intensity for landslide initiation is represented as a power-law function of rainfall duration. Permeable sandstone slopes have a greater critical rainfall and hence a longer recurrence interval than impermeable mudstone slopes. The longer recurrence interval of the threshold in the sandstone hillslopes implies a lower potential for landsliding, corresponding to lower landslide activity.

The rainfall thresholds in the present study incorporate site-specific factors, such as the

strength of slope materials and slope hydrological processes. The analytical procedure for determining the thresholds is applicable to any region where geotechnical soil properties and a certain amount of hydrological data are available.

Acknowledgements

Technical support by Dr. Tsuyoshi Hattanji (University of Tsukuba) made the continuous hydrological measurements possible. Discussions with members of the geomorphology research group of the University of Tsukuba helped motivate this work. This research was financially supported by the Science Research Fund of the Ministry of Education, Science and Culture (B-16300292, principal investigator: Y. Matsukura).

References

Caine N. 1980. The rainfall intensity–duration control of shallow landslides and debris flows. *Geografiska Annaler* **A62**: 23–27.

Cannon SH, Ellen S. 1985. Rainfall conditions for abundant debris avalanches, San Francisco Bay region, California. *California Geology* **38**: 267–272.

D'Odorico P, Fagherazzi S, Rigon R. 2005. Potential for landsliding: Dependence on hyetograph characteristics. *Journal of Geophysical Research* **110**: F01007. DOI: 10.1029/2004JF000127

Fannin RJ, Jaakkola J, 1999. Hydrological response of hillslope soils above a debris-slide headscarp. *Canadian Geotechnical Journal* **36**: 1111–1122.

Fannin RJ, Jaakkola J, Wilkinson JMT, Hetherington ED. 2000. Hydrologic response of soils to precipitation at Carnation Creek, British Columbia, Canada. *Water Resources Research* **36**: 1481–1494.

Furuya T, Ohkura H. 1992. Some geological and geomorphological characteristics of the slope failures on the Mt. Kano-zan and its environs in the Boso Peninsula, Japan. *Journal of Japan Landslide Society* **28**(4): 29–36 (in Japanese with English abstract).

Iida T. 2004. Theoretical research on the relationship between return period of rainfall and shallow landslides. *Hydrological Processes* **18**: 739–756. DOI: 10.1002/hyp.1264

Ito M. 1998. Submarine fan sequences of the lower Kazusa Group, a Plio–Pleistocene forearc basin fill in the Boso Peninsula, Japan. *Sedimentary Geology* **122**: 69–93.

Ito M, Horikawa K. 2000. Millennial- to decadal-scale fluctuation in the paleo-Kuroshio Current documented in the Middle Pleistocene shelf succession on the Boso Peninsula, Japan. *Sedimentary Geology* **137**: 1–8.

Iverson RM. 2000. Landslide triggering by rain infiltration. *Water Resources Research* **36**: 1897–1910.

Iwai S, Ishiguro M. 1970. *Applied Hydrological Statistics*. Morikita Shuppan: Tokyo (in Japanese).

Jakob M, Weatherly H. 2003. A hydroclimatic threshold for landslide initiation on the North Shore Mountains of Vancouver, British Columbia. *Geomorphology* **54**: 137–156. DOI: 10.1016/S0169-555X(02)00339-2

Johnson KA, Sitar N. 1990. Hydrologic conditions leading to debris-flow initiation. *Canadian Geotechnical Journal* **27**: 789–801.

Keefer DK, Wilson RC, Mark RK, Brabb EE, Brown WM, Ellen SD, Harp EL, Wieczorek GF, Alger CS, Zatkin RS. 1987. Real-time landslide warning during heavy rainfall. *Science* **238**: 921–925.

Kosugi K. 1994. Three-parameter lognormal distribution model for soil water retention. *Water Resources Research* **30**: 891–901.

Matsushi Y, Matsukura Y. 2004. Mechanism and location of slope failures in hilly terrains with different bedrock permeability. *Transactions, Japanese Geomorphological Union* **25**: 139–159 (in Japanese with English abstract).

Matsushi Y, Matsukura Y. 2006. Cohesion of unsaturated residual soils as a function of volumetric water content. *Bulletin of Engineering Geology and the Environment* **65**: 449–455. DOI: 10.1007/s10064-005-0035-9

Matsushi Y, Hattanji T, Matsukura Y. 2006. Mechanisms of shallow landslides on soil-mantled hillslopes with permeable and impermeable bedrocks in the Boso Peninsula, Japan. *Geomorphology* **76**: 92–108. DOI: 10.1016/j.geomorph.2005.10.003

Montgomery DR, Dietrich WE. 1994. A physically based model for the topographic control on shallow landsliding. *Water Resources Research* **30**: 1153–1171.

Reneau SL, Dietrich WE, Donahue DJ, Jull AJT, Rubin M. 1990. Late Quaternary history of colluvial deposition and erosion in hollows, central California Coast Ranges. *Geological Society of America Bulletin* **102**: 969–982.

Selby MJ. 1993. *Hillslope Materials and Processes, Second Edition*. Oxford University Press: Oxford.

Simoni A, Berti M, Generali M, Elmi C, Ghirotti M. 2004. Preliminary result from pore pressure monitoring on an unstable clay slope. *Engineering Geology* **73**: 117–128. DOI: 10.1016/j.enggeo.2003.12.004

Taylor JR. 1997. *An Introduction to Error Analysis: the Study of Uncertainties in Physical Measurements, Second Edition*. University Science Books: Mill Valley,

California.

Terlien MTJ. 1998. The determination of statistical and deterministic hydrological landslide-triggering thresholds. *Environmental Geology* **35**: 124–130.

Trustrum NA, De Rose RC. 1988. Soil depth–age relationship of landslides on deforested hillslopes, Taranaki, New Zealand. *Geomorphology* **1**: 143–160.

Van Genuchten MTh. 1980. A closed-form equation for predicting the hydraulic conductivity of unsaturated soils. *Soil Science Society of America Journal* **44**: 892–898.

Wieczorek GF. 1987. Effect of rainfall intensity and duration on debris flows in central Santa Cruz Mountains, California. In *Debris Flows/Avalanches: Process, Recognition, and Mitigation*, Costa JE, Wieczorek GF (eds). Reviews in Engineering Geology VII. Geological Society of America: 93–104.

Table I. Geotechnical properties of the soils

		Sandstone	Mudstone
Dry unit weight of soil γ_d (kN/m^3)		12·7	11·1
Porosity (m^3/m^3)		0·52	0·58
Grain-size distribution	Sand (%)	84·3	43·9
	Silt (%)	10·1	43·7
	Clay (%)	5·6	12·4
Permeability	Soil layer (m/s)	3–9×10^{-5}	8×10^{-6}–2×10^{-5}
	Bedrock (m/s)	6–7×10^{-5}	<5×10^{-8}
Shear strength parameters			
Dry soil cohesion *C* (kPa)		35·8	192·9
Strength reduction coefficient μ (–)		4·81	6·94
Angle of shearing resistance ϕ (°)		28·3	27·7

Table II. Parameter values for the soil-water retention characteristics

	Saturated v.w.c. θ_s (m^3/m^3)	**Residual v.w.c. θ_r (m^3/m^3)**	**Inflection point ψ_0 ($\times 10^{-2}$ m)**	**Fitting parameter m (–)**	**r^2**
Sandstone					
Depth 30 cm	0·47	0·17	−18·9	0·58	0·98
Depth 75 cm	0·47	0·16	−25·2	0·60	0·95
In situ envelope	0·47	0·16	−10·0	0·56	–
Mudstone					
Depth 15 cm	0·53	0·35	−5·7	0·47	0·95
Depth 30 cm	0·53	0·32	−0·1	0·20	0·99
In situ envelope	0·53	0·20	−5·0	0·20	–

v.w.c.: volumetric water content.

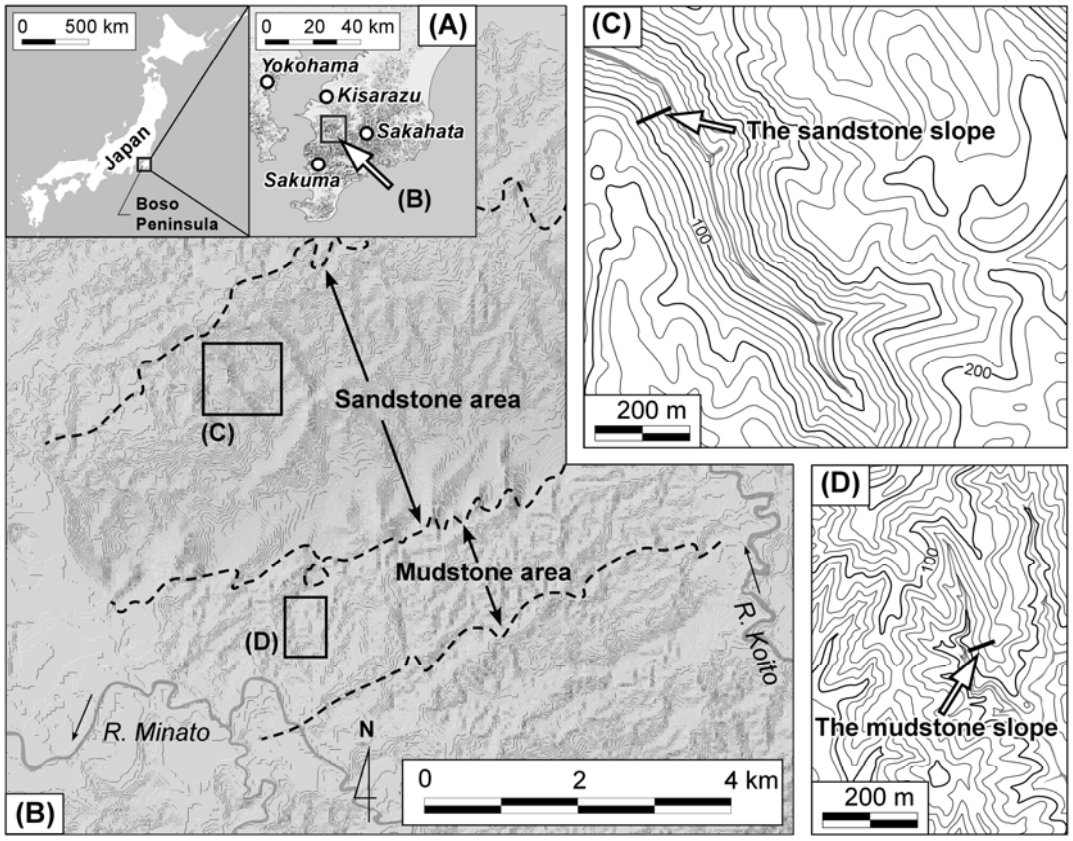
0 500 km
Japan
Boso Peninsula
0 20 40 km
(A)
Yokohama
Kisarazu
Sakahata
Sakuma
(B)
(C)
The sandstone slope
100
200
200 m
Sandstone area
(C)
Mudstone area
(D)
R. Koito
R. Minato
N
0 2 4 km
(B)
(D)
100
The mudstone slope
200 m

Fig. 1

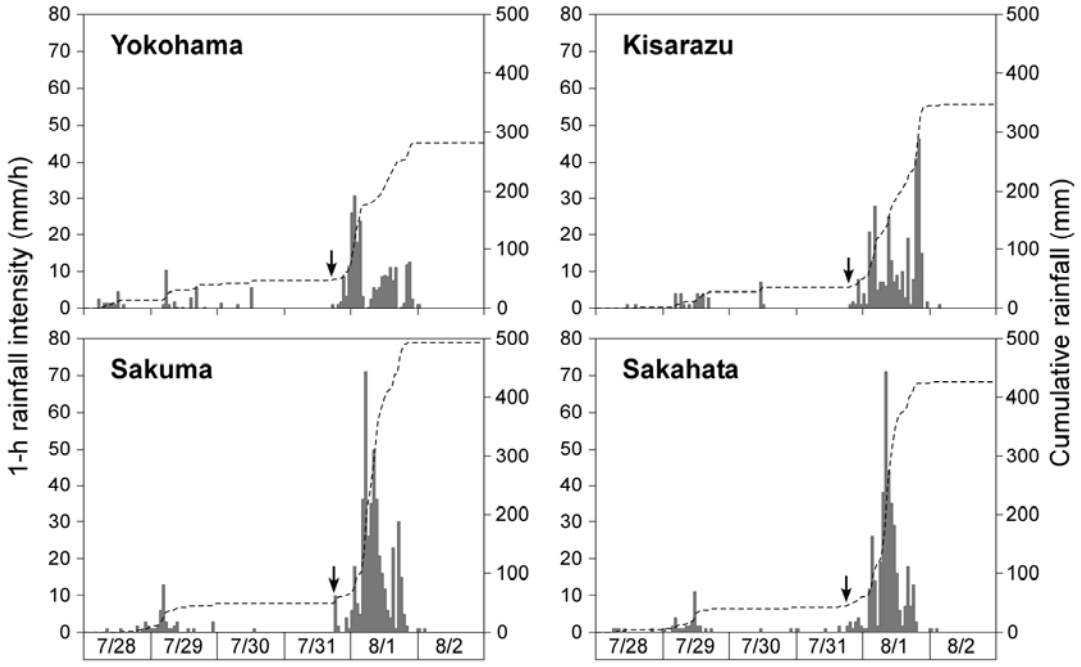
Yokohama
Kisarazu
Sakuma
Sakahata
1-h rainfall intensity (mm/h)
Cumulative rainfall (mm)
7/28
7/29
7/30
7/31
8/1
8/2

Fig. 2

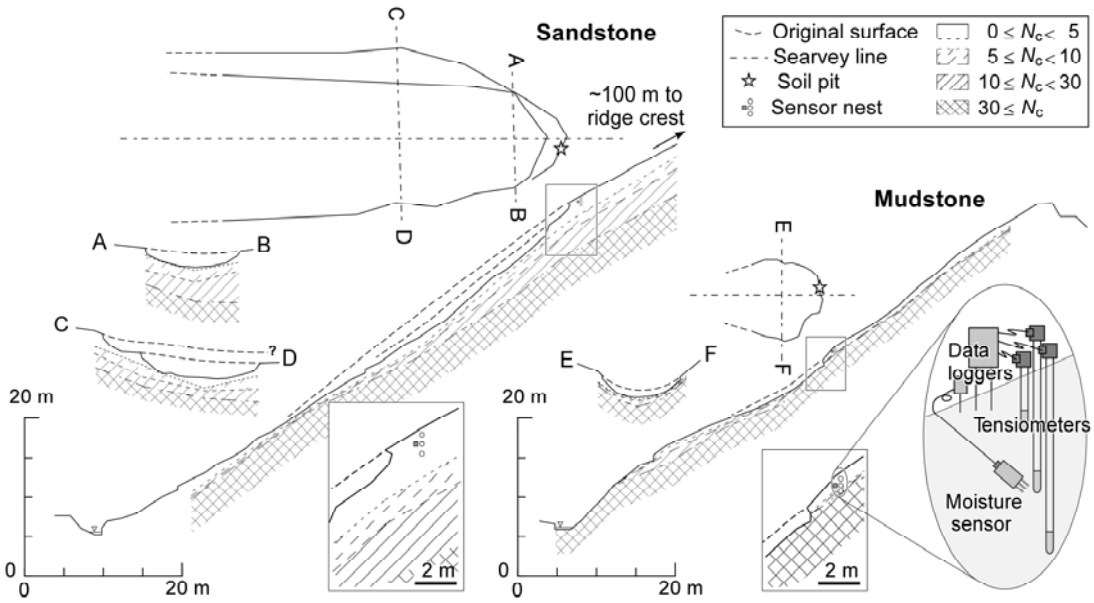
Sandstone
Mudstone
~100 m to ridge crest
Original surface
Searvey line
Soil pit
Sensor nest
0 ≤ Nc < 5
5 ≤ Nc < 10
10 ≤ Nc < 30
30 ≤ Nc
A
B
C
D
E
F
20 m
0
20 m
2 m
Data loggers
Tensiometers
Moisture sensor

Fig. 3

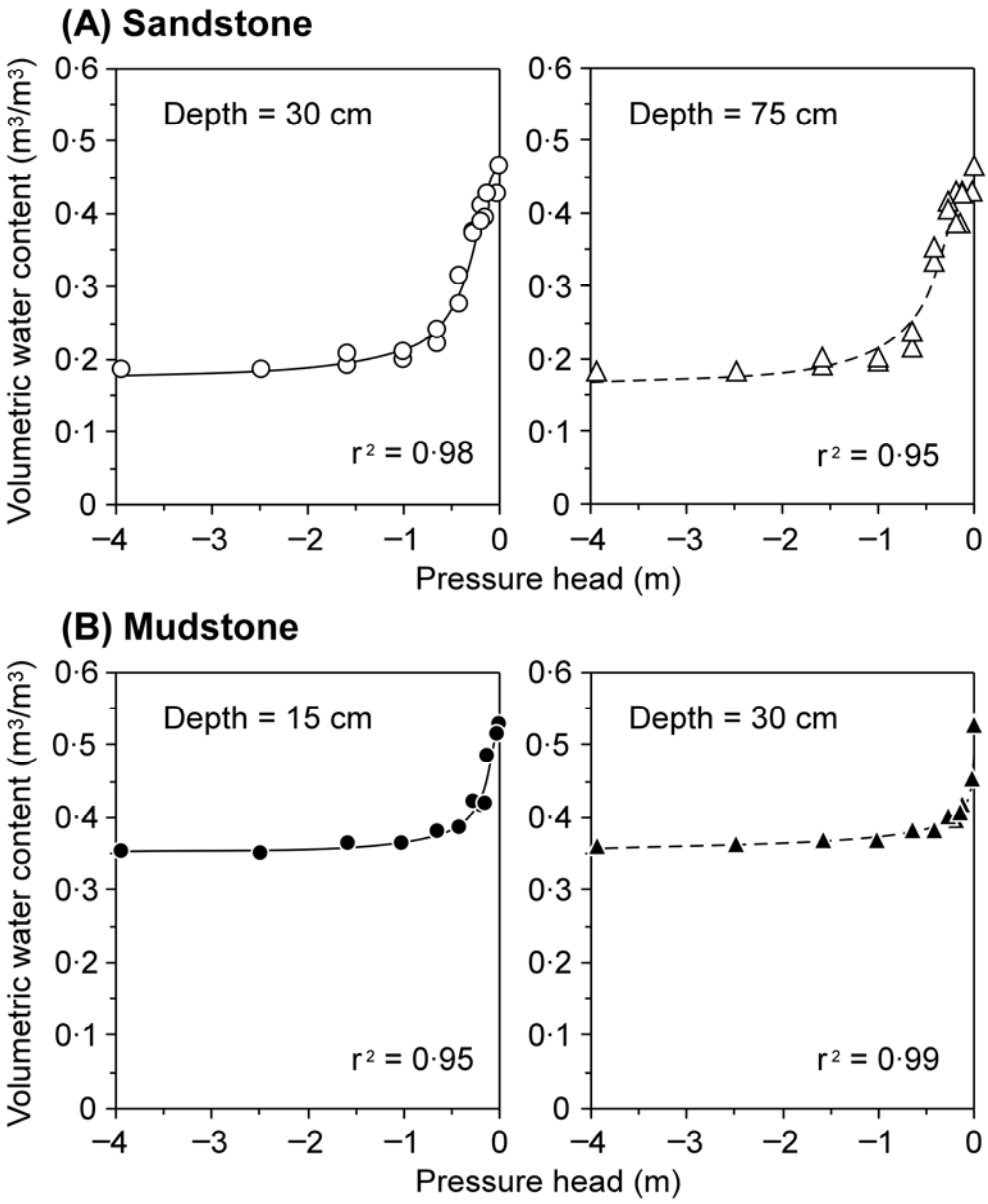
(A) Sandstone
Depth = 30 cm
Depth = 75 cm
r² = 0·98
r² = 0·95
Volumetric water content (m³/m³)
Pressure head (m)
(B) Mudstone
Depth = 15 cm
Depth = 30 cm
r² = 0·95
r² = 0·99
Volumetric water content (m³/m³)
Pressure head (m)

Fig. 4

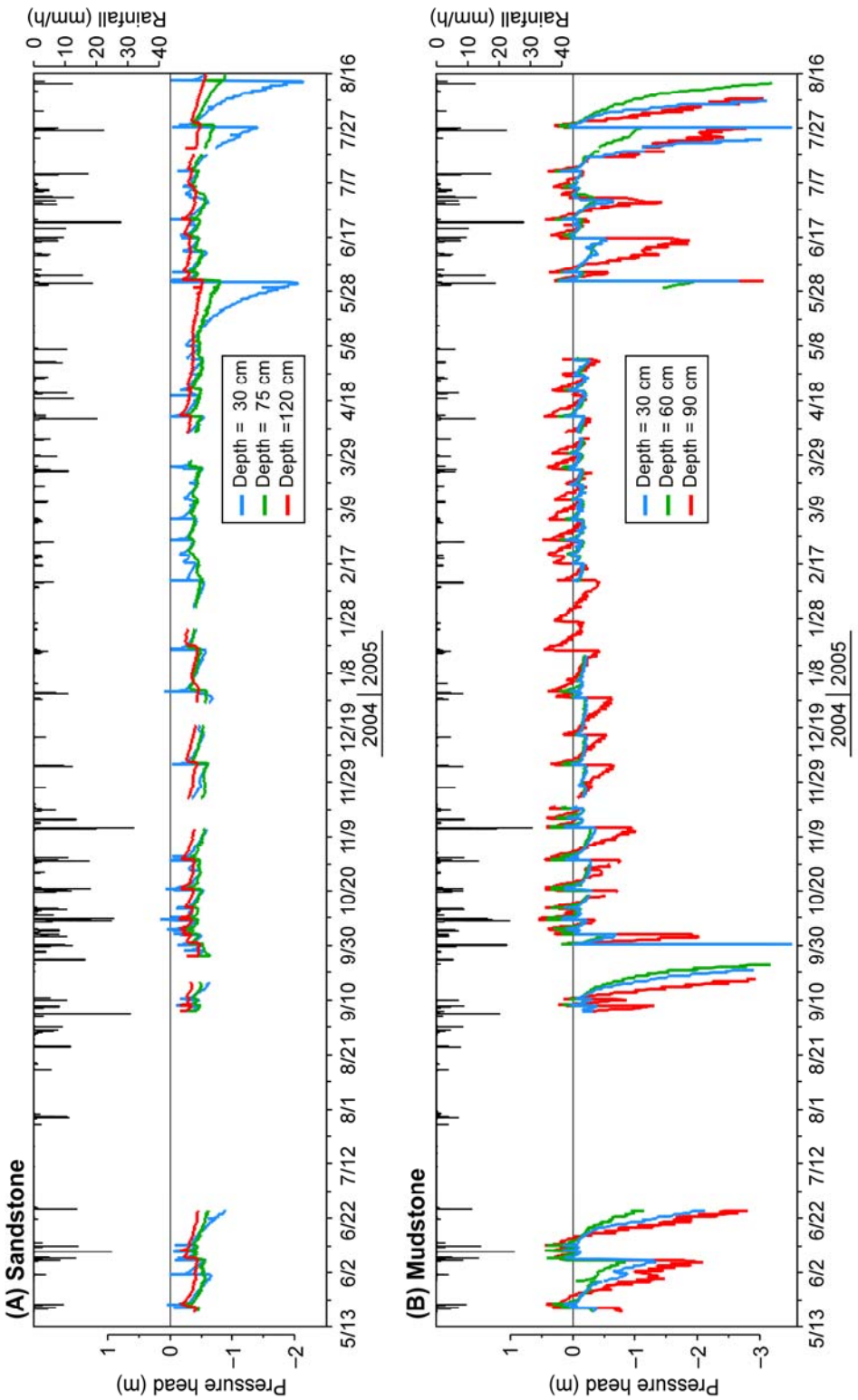
(A) Sandstone
Rainfall (mm/h)
0
10
20
30
40
Depth = 30 cm
Depth = 75 cm
Depth =120 cm
Pressure head (m)
1
0
−1
−2
5/13
6/2
6/22
7/12
8/1
8/21
9/10
9/30
10/20
11/9
11/29
12/19
1/8
1/28
2/17
3/9
3/29
4/18
5/8
5/28
6/17
7/7
7/27
8/16
2004
2005
(B) Mudstone
Rainfall (mm/h)
0
10
20
30
40
Depth = 30 cm
Depth = 60 cm
Depth = 90 cm
Pressure head (m)
1
0
−1
−2
−3
5/13
6/2
6/22
7/12
8/1
8/21
9/10
9/30
10/20
11/9
11/29
12/19
1/8
1/28
2/17
3/9
3/29
4/18
5/8
5/28
6/17
7/7
7/27
8/16
2004
2005

Fig. 5

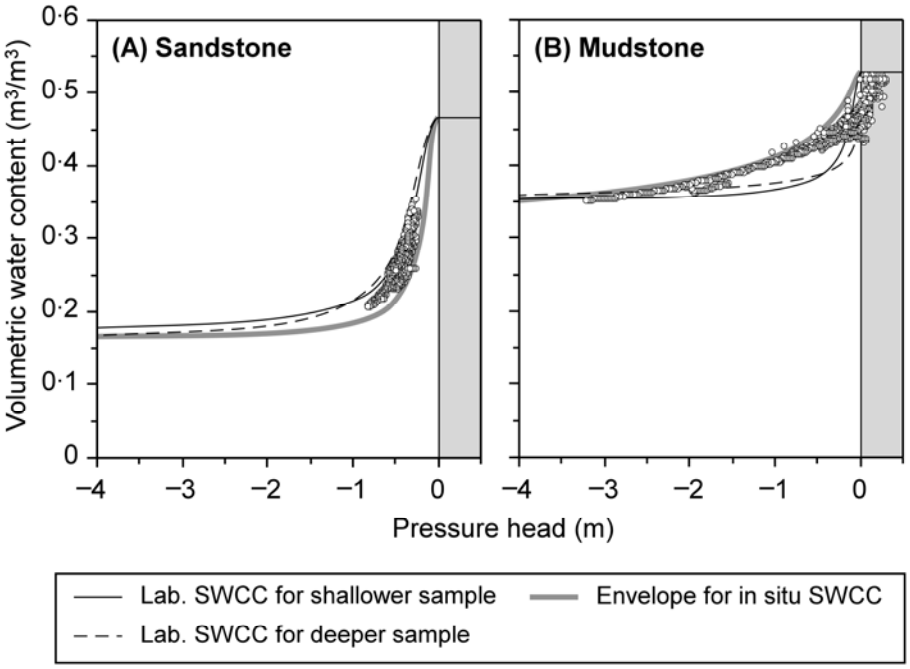
(A) Sandstone
(B) Mudstone
Volumetric water content (m³/m³)
0·6
0·5
0·4
0·3
0·2
0·1
0
−4
−3
−2
−1
0
Pressure head (m)
Lab. SWCC for shallower sample
Lab. SWCC for deeper sample
Envelope for in situ SWCC

Fig. 6

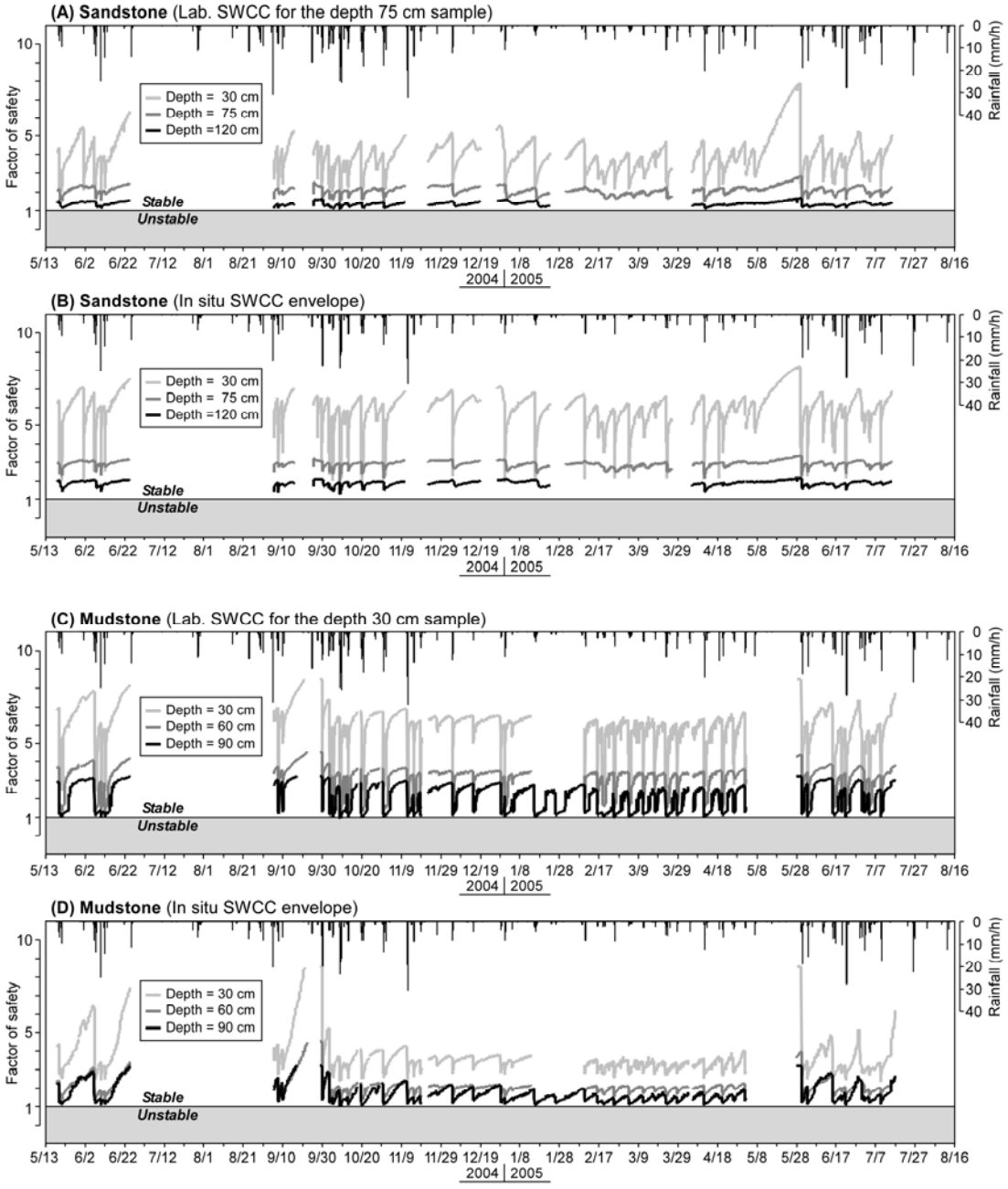
(A) Sandstone (Lab. SWCC for the depth 75 cm sample)
Depth = 30 cm
Depth = 75 cm
Depth =120 cm
Stable
Unstable
Factor of safety
Rainfall (mm/h)
(B) Sandstone (In situ SWCC envelope)
Depth = 30 cm
Depth = 75 cm
Depth =120 cm
Stable
Unstable
Factor of safety
Rainfall (mm/h)
(C) Mudstone (Lab. SWCC for the depth 30 cm sample)
Depth = 30 cm
Depth = 60 cm
Depth = 90 cm
Stable
Unstable
Factor of safety
Rainfall (mm/h)
(D) Mudstone (In situ SWCC envelope)
Depth = 30 cm
Depth = 60 cm
Depth = 90 cm
Stable
Unstable
Factor of safety
Rainfall (mm/h)
5/13 6/2 6/22 7/12 8/1 8/21 9/10 9/30 10/20 11/9 11/29 12/19 1/8 1/28 2/17 3/9 3/29 4/18 5/8 5/28 6/17 7/7 7/27 8/16
2004 2005

Fig. 7

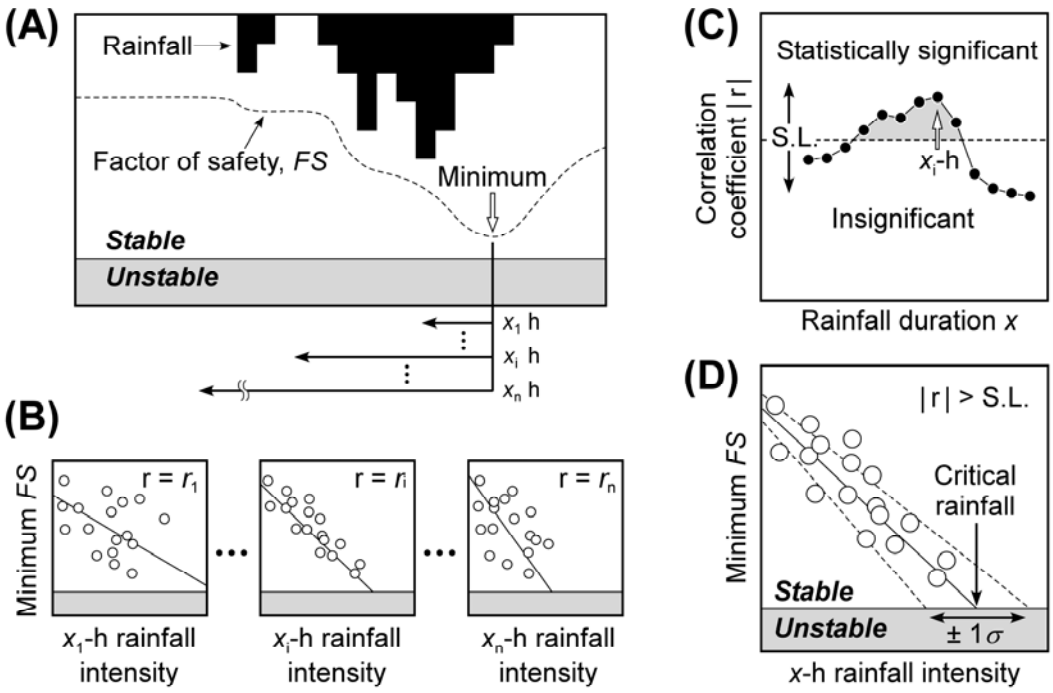
(A)
Rainfall
Factor of safety, FS
Minimum
Stable
Unstable
x1 h
xi h
xn h
(B)
Minimum FS
r = r1
r = ri
r = rn
x1-h rainfall intensity
xi-h rainfall intensity
xn-h rainfall intensity
(C)
Statistically significant
Correlation coefficient | r |
S.L.
xi-h
Insignificant
Rainfall duration x
(D)
| r | > S.L.
Minimum FS
Critical rainfall
Stable
Unstable
± 1σ
x-h rainfall intensity

Fig. 8

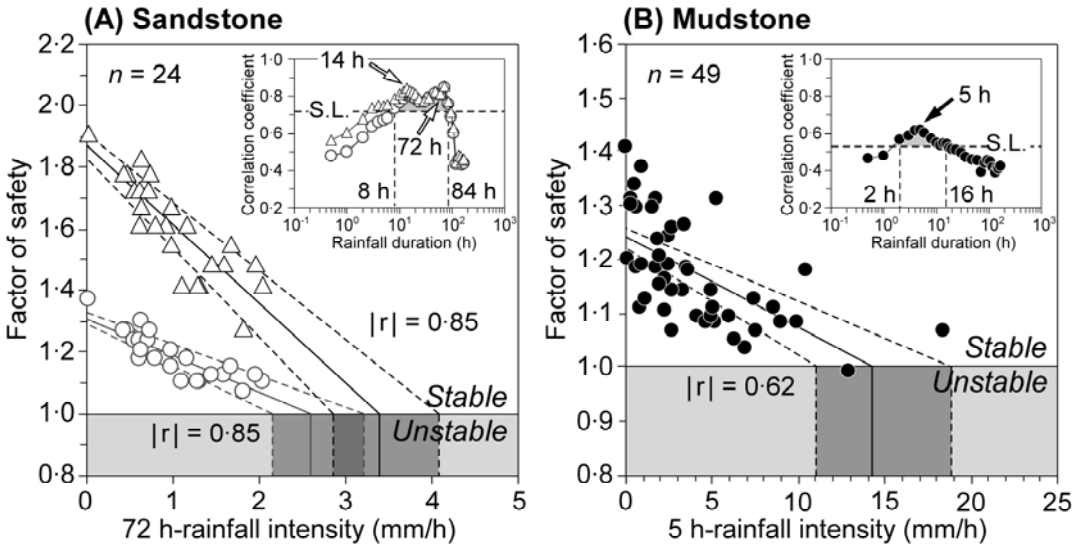
(A) Sandstone
n = 24
14 h
S.L.
72 h
8 h
84 h
Correlation coefficient
Rainfall duration (h)
|r| = 0·85
Stable
Unstable
|r| = 0·85
Factor of safety
72 h-rainfall intensity (mm/h)
(B) Mudstone
n = 49
5 h
S.L.
2 h
16 h
Correlation coefficient
Rainfall duration (h)
Stable
Unstable
|r| = 0·62
Factor of safety
5 h-rainfall intensity (mm/h)

Fig. 9

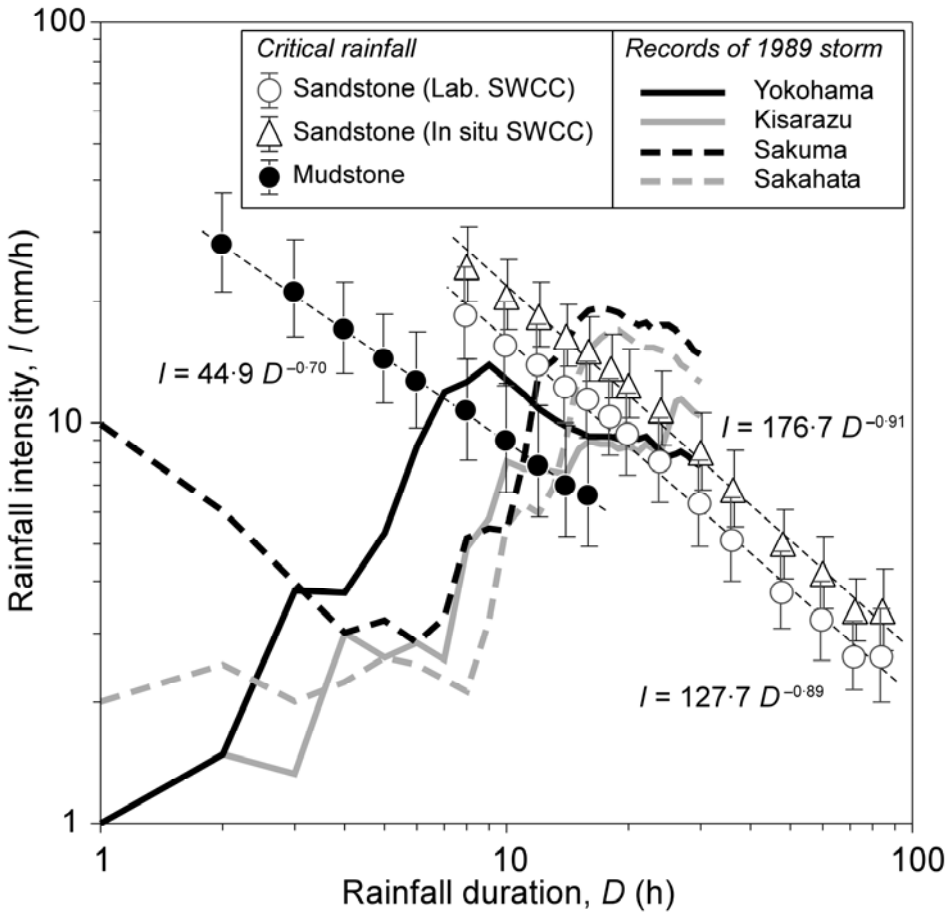
Critical rainfall
Sandstone (Lab. SWCC)
Sandstone (In situ SWCC)
Mudstone
Records of 1989 storm
Yokohama
Kisarazu
Sakuma
Sakahata
I = 44·9 D^−0·70
I = 176·7 D^−0·91
I = 127·7 D^−0·89
Rainfall intensity, I (mm/h)
Rainfall duration, D (h)
100
10
1
1
10
100

Fig. 10

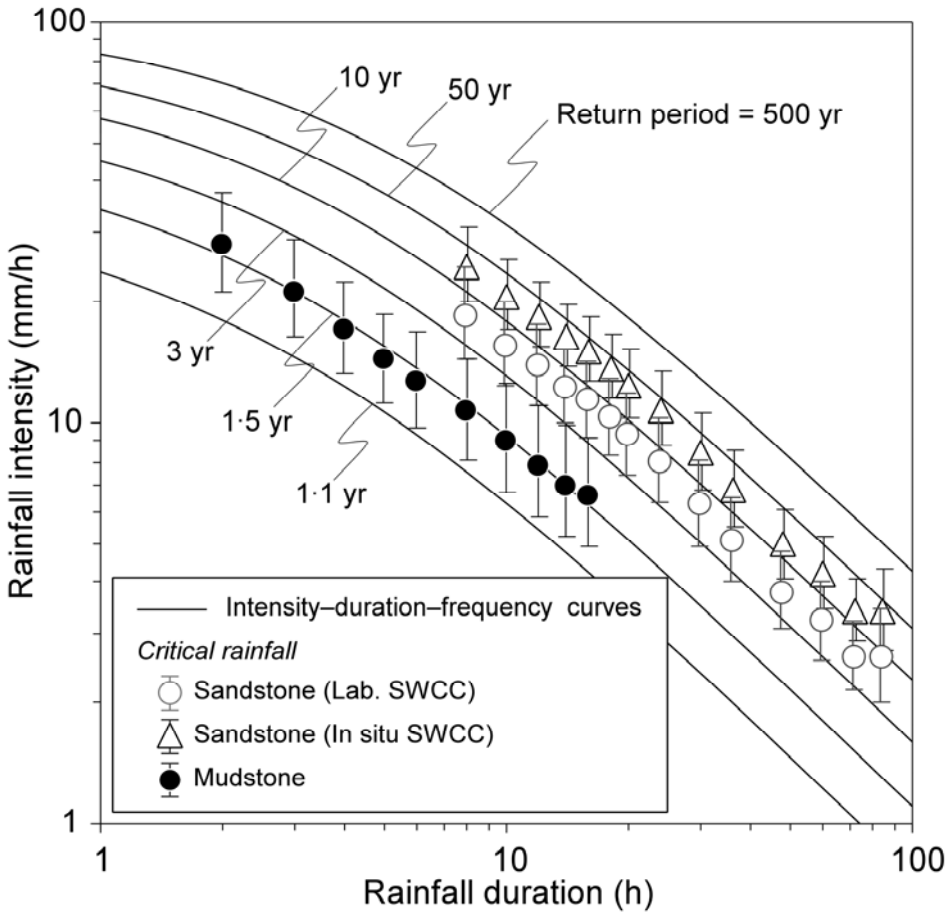
100
10
1
Rainfall intensity (mm/h)
1
10
100
Rainfall duration (h)
10 yr
50 yr
Return period = 500 yr
3 yr
1·5 yr
1·1 yr
Intensity–duration–frequency curves
Critical rainfall
Sandstone (Lab. SWCC)
Sandstone (In situ SWCC)
Mudstone

Fig. 11

Figure legends

Figure 1. Topography of the study area and locations of the selected slopes.

Figure 2. Records of the 1989 storm at the four meteorological stations. The locations of these stations are shown in Figure 1A. Bars show 1-h rainfall intensity, broken curves represent cumulative rainfall. Arrows indicate the onset of the main storm body.

Figure 3. Profiles of the selected slopes, and plan views and cross sections of slip scars. The locations of these two sites are shown in Figure 1C and D. The subsurface soil layers are inferred from soil soundings. Enlarged views show the nests of sensors for hydrological monitoring.

Figure 4. Soil-water characteristic curves of the soils. The plots represent drying soil-water retention from saturated conditions. The broken and solid lines are best-fit Kosugi's (1994) model curves (see Equation 2 in text), whose optimum parameter values are listed in Table 2.

Figure 5. Pressure head fluctuations in response to rainfall in the sandstone (A) and mudstone (B) slopes.

Figure 6. Soil-water retention plots from in situ monitoring. SWCC: soil-water characteristic curve. The solid and broken lines indicate the best-fit model curves for the laboratory data (cf. Figure 4). The gray lines show the lower (for sandstone) and upper

(for mudstone) envelope for the in situ data.

Figure 7. Slope stability fluctuations calculated from observed pressure heads. SWCC: soil-water characteristic curve. Both the laboratory and in situ parameter-sets for SWCCs were used for the calculation.

Figure 8. Analytical procedures for determining critical rainfall. (A) Schematic illustrating a dip in the factor of safety and time frames for the preceding rainfall durations. The shaded unstable regions are defined as the range of factors of safety below unity. (B) Sequential correlation analysis between the minimum factor of safety and mean rainfall intensity during a given duration. (C) Identification of effective rainfall durations. A significance level, S.L., determines statistically-meaningful correlations. (D) Definition of the critical rainfall intensities. Solid and broken lines indicate linear-regression lines with 68% confidence limits.

Figure 9. Inverse correlations between the minimum factors of safety and mean rainfall intensities at the most effective rainfall durations. Insets show the changes in the correlation coefficient against varying time-frames of rainfall duration. Open circles in the correlation for sandstone indicate the results from the laboratory soil-water characteristic curve (depth 75 cm, Figure 4A); triangles show the results using the in situ envelope (Figure 6A). Solid and broken lines indicate linear-regression lines with 68% confidence limits (cf. Figure 8D).

Figure 10. Rainfall thresholds for landsliding and temporal changes in mean rainfall

intensity of the torrential rainfall on August 1, 1989. SWCC: soil-water characteristic curve. Error bars of the critical rainfall represent 68% confidence limits from the linear-regression analysis (cf. Figure 8D). The four bold lines were computed from the rainfall records of the 1989 storm (Figure 2), by dividing the cumulative rainfall with elapsed time from the onset of the storm body.

Figure 11. Recurrence intervals of critical rainfall. SWCC: soil-water characteristic curve. The intensity–duration–frequency curves were computed from the annual records of the most intensive 1-h and 1-day rainfalls from 1940 to 2004 at Yokohama meteorological station (cf. Figure 1A).